A&A 396, 269–281 (2002)
DOI: 10.1051/0004-6361:20021396

Astronomy & Astrophysics

Effects of the heliospheric interface on the interplanetary Lyman α glow seen at 1 AU from the Sun

E. Quémerais[1] and V. Izmodenov[2]

[1] Service d'Aéronomie du CNRS, BP 3, 91371, Verrières le Buisson, France
[2] Institute for Problems in Mechanics, Moscow, Russia
e-mail: izmod@ipmnet.ru

Received 12 November 2001 / Accepted 9 September 2002

Abstract. This work presents multiple scattering computations of interplanetary background line profiles using Angle Dependent Partial Frequency Redistribution to model the scattering process as explained by Quémerais (2000). The density and velocity distribution of hydrogen atoms in the heliosphere was computed using a self-consistent model of the solar wind interaction with the two-component (H atoms and plasma) interstellar plasma (Izmodenov et al. 2001).
We show that the main difference of the heliospheric interface model as compared to the classical hot model lies in the existence of three populations of H atoms in the heliosphere. These populations are primary interstellar atoms, secondary interstellar atoms created by charge exchange in the outer heliosheath and a hot component (around 150 000 K) created in the inner heliosheath. The two interstellar components provide additional asymmetry in the backscattered Lyα profile at 1 AU, which is not expected from the classical hot model. At the Earth orbit in the upwind direction, the hot component of the backscattered intensity represents less than 5% of the total intensity. It reaches 15% in the downwind direction.
Although the heliospheric interface has some effect on the upwind to downwind ratio of total backscattered Lyα intensity, on the apparent velocity and apparent temperature of interplanetary line profiles, they are difficult to discriminate from the results of the variations of the solar parameters. Therefore our following models should include time-dependence effects on the interplanetary hydrogen distribution.
Finally, it is concluded that measurements of interplanetary Lyα profiles in the inner heliosphere may serve as a good diagnostic of the heliospheric interface. The existence of a faint hot component in the Lyman α backscattered profiles would serve as a new tool to study the heliospheric interface.

Key words. interplanetary medium – radiative transfer

1. Introduction

The interplanetary Lyman α glow was first observed in the late 1960s and identified as an interplanetary emission in the early 1970s (Thomas & Krassa 1971; Bertaux & Blamont 1971). The study of the spatial distribution of the hydrogen atoms which are the source of this UV glow in the interplanetary medium has led to various interesting results. The early studies on the interplanetary glow are reviewed by Ajello et al. (1987).

In 2002, there are at least five UV photometers or spectrometers in the interplanetary medium that can study the interplanetary Lyman α glow. The oldest is UVS on Voyager 1 launched in 1977 (Broadfoot et al. 1977). At its present position, more than 80 AU from the Sun, UVS/Voyager 1 gives an unprecedented view of the interplantary glow in the outer heliosphere. SWAN on SOHO was designed to study the interplanetary glow and its variations with solar cycle. Its was launched in December 1995 (Bertaux et al. 1995). Other spectrometers were designed to study planetary atmospheres but are also able to study the interplanetary UV emissions. UVS on Galileo was launched in the early 1990s and is still operating (Hord et al. 1992). UVS on NOZOMI (Fukunishi et al. 1999) has also studied the interplanetary glow. Finally, high resolution line profile measurements of the interplanetary Lyman α emission have been performed by GHRS on HST (Clarke et al. 1998).

Costa et al. (1999), using the SWAN/SOHO hydrogen cell data, have found that the temperature of the interplanetary hydrogen at large distances from the sun (say 50 AU) is significantly larger than the value estimated for the gas in the Local Interstellar Medium. Moreover, the bulk velocity inferred from their study is around 20 or 21 km s^{-1} at 50 AU, which is lower than the 26 km s^{-1} relative velocity between the Sun and the

Send offprint requests to: E. Quémerais,
e-mail: eric.quemerais@aerov.jussieu.fr

Local Interstellar Gas. It has been suggested that these results prove that the interstellar hydrogen atoms are heated and decelerated when crossing the region that constitutes the boundary, or interface, between the expanding solar wind and the ionized component of the interstellar gas. Because of coupling processes through charge exchange between protons and hydrogen atoms, the hydrogen atom velocity distribution is actually modified when crossing the region of the heliospheric interface.

Modeling this interface is a very difficult task. It is even more complex when effects of proton-neutral hydrogen coupling are taken into account. Baranov & Malama (1993) first published hydrogen distributions deduced from a self-consistent computation of the plasma-neutral atoms coupling at the heliospheric interface. These authors showed that the hydrogen distribution is significantly different from the simple results of the hot model (Thomas 1978; Lallement et al. 1985) which assumes a simple Gaussian distribution of the gas in the outer heliosphere. More recently, Izmodenov et al. (1999) have studied in detail the results of interstellar hydrogen filtration at the heliospheric interface in the frame work of the two-shock model developed by Baranov & Malama (1993).

The hydrogen distribution in the inner heliosphere is mainly influenced by ionization processes from the Sun. However, effects of the interface imprinted on the distribution at large distances from the Sun will remain because of the very large mean free path of the hydrogen atoms in the interplanetary medium.

Studying the interplanetary glow data requires one to model the scattering process of the Lyman α photons in the interplanetary medium. The scattering of a single photon can be accurately described by the Angle Dependent Partial Frequency Redistribution (ADPFR) function which relates the energy of the incoming and outgoing photons with the velocity of the scatterer and the scattering angle. A model based on a Monte Carlo scheme to represent this function for large numbers of photons was developed by Quémerais (2000) and applied to hydrogen velocity distributions derived from hot model calculations, i.e. without heliospheric interface effects. These calculations allowed then to derive line shifts and line widths of the interplanetary glow which is impossible in the case of the simpler hypothesis of Complete Frequency Redistribution (CFR).

In this paper, we present the results of ADPFR radiative transfer computations including hydrogen velocity distributions derived from the two-shock heliospheric interface model.

After reviewing the most significant aspects of the modeling, we present the results obtained for an observer at 1 AU from the Sun. An obvious application concerns the data of the Lyman α photometer on-board SOHO (Bertaux et al. 1995).

The aim of this work is to characterize the differences between Hot Model and Heliospheric Interface model results and their possible application to existing data sets.

In future works, the results presented here will be tested on actual spectral measurements of the interplanetary background obtained by the STIS/HST instrument. Hydrogen cell measurements of the SWAN/SOHO instrument (Quémerais et al. 1999) will also be used.

2. Model description

2.1. Hydrogen distributions

The interaction of the solar wind with the interstellar medium influences the distribution of interstellar atoms inside the heliosphere. At the present time, there is no doubt that the Local Interstellar Cloud is partly ionized. The plasma component of the LIC interacts with the solar wind plasma and forms the heliospheric interface (Fig. 1). Interstellar H atoms interact with the plasma component by charge exchange. This interaction strongly influences both plasma and neutral components. The main difficulty in the modeling of the H atom flow in the heliospheric interface is its kinetic character due to the large, i.e. comparable to the size of the interface, mean free path of H atoms with respect to the charge exchange process. In this paper, to get the H atom distribution in the heliosphere and heliospheric interface structure we use the self-consistent model developed by Baranov & Malama (1993). The kinetic equation for the neutral component and the hydrodynamic Euler equations were solved self-consistently by the method of global interactions. To solve the kinetic equation for H atoms, an advanced Monte Carlo method with splitting of trajectories (Malama 1991) was used. Basic results of the model were reported by Baranov & Malama (1995), Izmodenov et al. (1999), Izmodenov (2000), Izmodenov et al. (2001).

Hydrogen atoms newly created by charge exchange have the velocities of their ion partners in charge exchange collisions. Therefore, the parameters of these new atoms depend on the local plasma properties. It is convenient to distinguish four different populations of atoms depending on where in the heliospheric interface they originated. Population 1 corresponds to the atoms created in the supersonic solar wind. It is denoted SSWA (supersonic solar wind atoms). Population 2 (denoted HSWA, hot solar wind atoms) represents the atoms originating in the heliosheath. Population 3 (HIA, hot interstellar atoms) are the atoms created in the disturbed interstellar wind. We will call original (or primary) interstellar atoms population 4 (PIA, primary interstellar atoms). The number densities and mean velocities of these populations are shown in Fig. 2 as functions of the heliocentric distance. The main results of the model for the H atom populations can be summarized as follows:

PIAs are significantly filtered (i.e. their number density is reduced) before reaching the termination shock. Since slow atoms have a smaller mean free path compared to fast atoms, they undergo more charge exchange. This kinetic effect, called *selection*, results in a deviation of the interstellar distribution function from Maxwellian (Izmodenov et al. 2001). The selection also results in ~10% increase of the primary atom mean velocity at the termination shock (Fig. 2C).

HIAs are created in the disturbed interstellar medium by charge exchange of primary interstellar neutrals and protons decelerated by the bow shock. The secondary interstellar atoms collectively make up the *H wall*, a density increase at the heliopause. The H wall has been predicted by Baranov et al. (1991) and detected toward α Cen (Linsky & Wood 1996). At the termination shock, the number density of the secondary

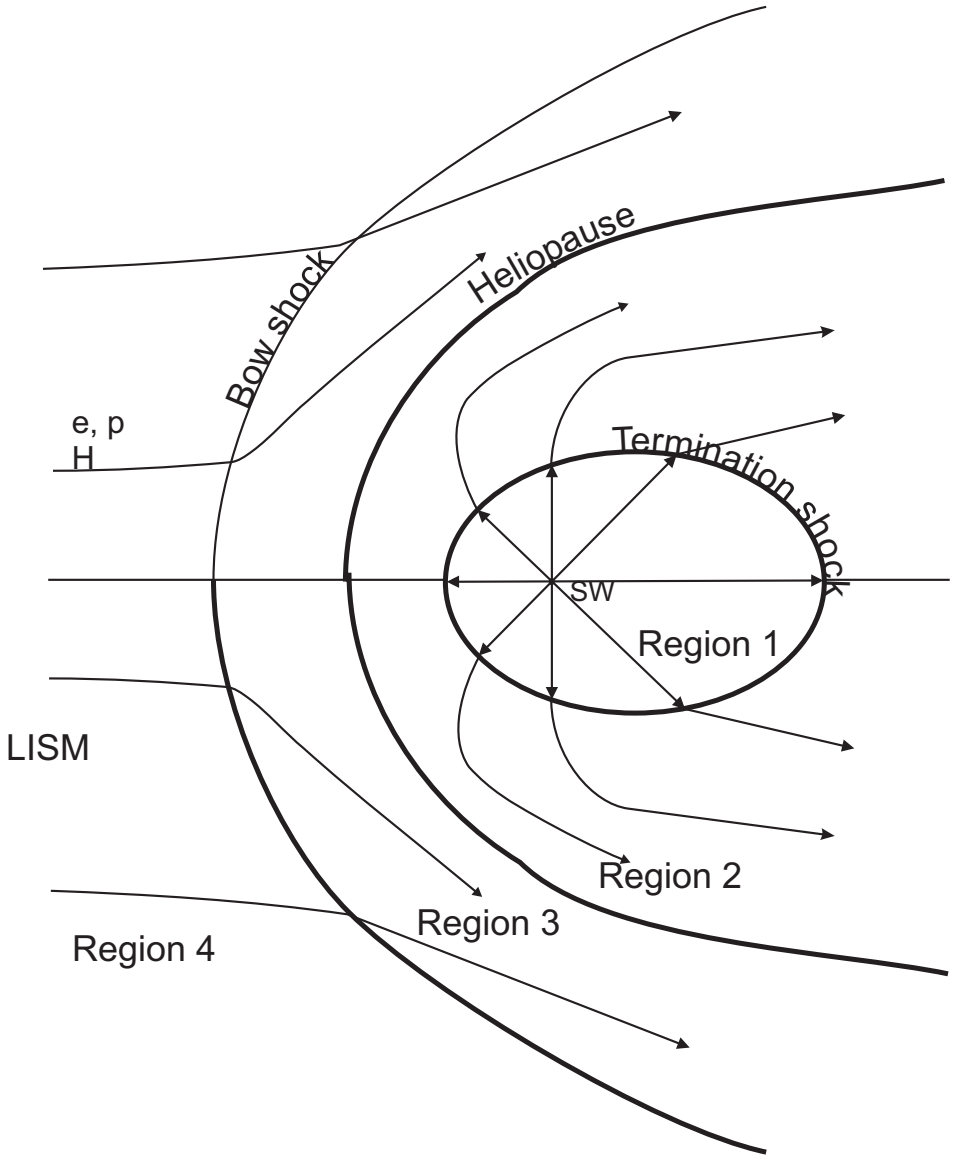

Fig. 1. The heliospheric interface is the region of the solar wind interaction with LIC. The heliopause is a contact discontinuity, which separates the plasma wind from interstellar plasmas. The termination shock decelerates the supersonic solar wind. The bow shock may also exist in the interstellar medium. The heliospheric interface can be divided into four regions with significantly different plasma properties: 1) supersonic solar wind; 2) subsonic solar wind in the region between the heliopause and termination shock; 3) disturbed interstellar plasma region (or "pile-up" region) around the heliopause; 4) undisturbed interstellar medium.

neutrals is comparable to the number density of the primary interstellar atoms (Fig. 2A, dashed curve). The relative abundances of PIAs and HIAs entering the heliosphere depends on the degree of ionization in the interstellar medium. It has been shown by Izmodenov et al. (1999) that the relative abundance of HIAs inside the termination shock increases with increasing interstellar proton number density. The bulk velocity of HIAs is about 18–19 km s^{-1}. This population approaches the Sun. The velocity distribution of HIAs is not Maxwellian. The velocity distributions of different populations of H atoms were calculated in Izmodenov et al. (2001) for different directions from upwind. The fine structures of the velocity distribution of the primary and secondary interstellar populations vary with direction. These variations of the velocity distributions reflect the geometrical pattern of the heliospheric interface. The velocity distributions of the interstellar atoms can provide a good diagnostic of the global structure of the heliospheric interface.

The third component of the heliospheric neutrals, HSWAs, corresponds to the neutrals created in the heliosheath from hot and compressed solar wind protons. The number density of this population is an order of magnitude smaller than the number densities of the primary and secondary interstellar atoms. This population has a minor importance for interpretations of Ly α and pickup ion measurements inside the heliosphere. However, some of these atoms may probably be detected by Lyα hydrogen cell experiments due to their large Doppler shifts. Due to their high energies, the particles influence the plasma distributions in the LIC. Inside the termination shock the atoms

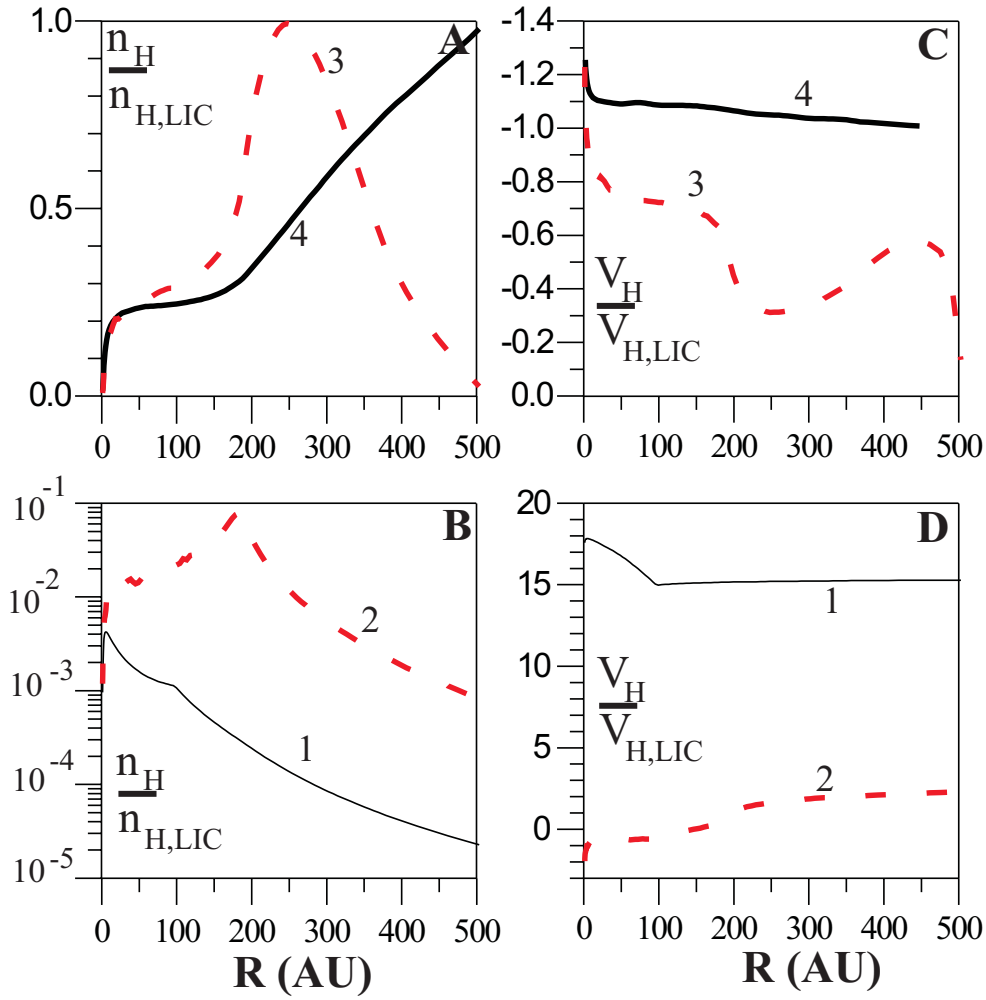

Fig. 2. Number densities and velocities of four populations of H atoms as functions of heliocentric distance in the upwind direction. 1 designates atoms created in the supersonic solar wind, 2 atoms created in the heliosheath (SSWAs), 3 atoms created in the disturbed interstellar plasma (HIAs), and 4 original (or primary) interstellar atoms (PIAs). Number densities are normalized to $n_{\mathrm{H,LIC}}$, velocities are normalized to V_{LIC}. It is assumed that $n_{\mathrm{H,LIC}} = 0.2$ cm^{-3}, $n_{\mathrm{p,LIC}} = 0.04$ cm^{-3}.

propagate freely. Thus, these atoms can be a source of information on the plasma properties in the place of their birth, i.e. the heliosheath.

The last population of heliospheric atoms is SSWAs, the atoms created in the supersonic solar wind. The number density of this atom population has a maximum at ~5 AU from the sun. At this distance, the number density of population 1 is about two orders of magnitude smaller that the number density of the interstellar atoms. Outside the termination shock the density decreases faster than $1/r^2$ where r is the heliocentric distance (curve 1, Fig. 2B). The mean velocity of population 1 is about 450 km s^{-1}, which corresponds to the bulk velocity of the supersonic solar wind. The *supersonic* atom population results in the plasma heating and deceleration upstream of the bow shock. This leads to the decrease of the Mach number ahead of the bow shock.

SSWAs velocities are Doppler shifted out of the solar H Lyman α line and therefore are not detectable in by interplanetary Lyman α measurements. Atoms of the three other populations penetrate the heliosphere and may backscatter solar Lyα photons. This is in contrast to the classical hot model (Thomas 1978; Lallement et al. 1985) which assumed that at large heliocentric distance the velocity distribution is Maxwellian and unperturbed by the heliospheric interface interaction.

Table 1 gives a summary of the different H populations in the heliosphere. The number of the region of origin of each population, as shown in Fig. 1, is also given in the table. We also give the range of variation of the number density of the population in the inner heliosphere as shown in Fig. 2.

In what follows, we will include the full distribution of the three populations (2, 3 and 4 from Table 1) that can actually backscatter solar Lyman α photons to compute the interplanetary UV background. Each population will be referred to by use of its label (PIA, HIA, HSWA). The hydrogen distribution model will be called three population model, denoted 3p model, because the SSWA is invisible to Lyα light.

Table 1. H populations summary.

Acronym	Full name	scatter H Ly-a	Origin	Nh/Nlic Range
SSWA	Supersonic Solar Wind Atoms	No	Region 1	10^{-3}–10^{-2}
HSWA	Hot Solar Wind Atoms	Yes	Region 2	10^{-3}–10^{-1}
HIA	Hot Interstellar Atoms	Yes	Region 3	0.1–0.3
PIA	Primary Interstellar Atoms	Yes	Region 4	0.1–0.3

For reference, the parameters of the hydrogen distribution model are given by

LIC parameters

Proton number density	0.04 cm^{-3}
Hydrogen number density	0.2 cm^{-3}
Bulk velocity	25 $km\,s^{-1}$
Temperature	5700 K

Solar parameters

Radiation pressure to gravitation (μ)	0.75
Proton number density at Earth	7 cm^{-3}
Solar wind velocity	450 $km\,s^{-1}$

2.2. Multi-component radiative transfer calculations

2.2.1. Radiative transfer model assumptions

In this study we use the results of two radiative transfer models following the scheme described by Quémerais (2000). Our method combines a standard iterative computation of the first-order and second-order scattering terms with Monte Carlo simulations used to compute the higher orders of scattering (i.e., photons that are scattered more than two times). The second-order scattering term is computed by integration over the whole sky of the first-order component. It is also computed independently by the Monte Carlo simulation. This provides a way to check the validity of both methods (Quémerais 2000).

The iterative scheme, i.e. computing order n_s from integration over the whole sky of terms of scattering order $n_s - 1$, could theoretically be applied to any order (see Sect. 2.3 of Quémerais 2000). However, starting from $n_s = 3$, it is much more efficient to use a Monte Carlo approach.

The general assumptions of our model are the following:

- The photon source frequency profile is derived from the SUMER/SOHO measurements (Lemaire et al. 1998). The source profile is shown in Quémerais (2000).
- The density distribution of the three populations is symmetrical around the wind axis going through sun center.
- The local distribution of hydrogen atoms is represented by the sum of three components.
- In each point of the heliosphere, the local distribution of each component is described by 6 values: a number density, a mean velocity and three temperatures which are the temperatures of the velocity distribution projected on the three directions of the local frame. These three temperatures can be different, which means that the local distribution is not necessarily a Maxwell-Boltzman distribution.
- The scattering process is computed following the Angle Dependent Partial Frequency Redistribution (Mihalas 1970). This means that the frequency of the outgoing photons depends on the frequency of the incoming photons, the scattering angle and the velocity distribution at the point of scattering. The numerical expressions of the redistribution function is given in Quémerais (2000).
- The scattering redistribution function includes the phase function given by Brandt & Chamberlain (1959). The improved phase function by Brasken & Kyrölä (1998) has not been included here because it leads to changes which are much lower than the expected accuracy of our Monte Carlo computation.

The Monte Carlo model has the following boundary conditions

- The solar photons are randomly generated following the solar H Lyman α line profile of Lemaire et al. (1998). The source is spatially isotropic.
- For each scattering, the new frequency of the photon is randomly generated using the ADPFR redistribution function and the local hydrogen distribution parameters at the point of scattering.
- There is no limit for the number of scatterings.
- The model stops following a photon once it has reached a distance of 600 AU from the Sun. This limit was obtained by comparison of different MC runs. It was shown that increasing this distance has no effect on the emissivity within 100 AU from the Sun.

Previous works have used the assumption of Complete Frequency Redistribution (Keller et al. 1981; Hall 1992; Quémerais & Bertaux 1993), for which the frequency of the outgoing photon only depends on the local density distribution at the point of scattering. Unfortunately, this simpler assumption does not allow for an exact computation of backscattered line profiles because it neglects of the incoming photon frequency profile. This applies to a medium with large optical thickness where many scatterings occur, not in the inner heliosphere. To be able to compute exact line profiles, we had to implement a scheme based on the actual Angle Dependent Partial Redistribution Function described by Mihalas (1970). Quémerais (2000) has devoted a whole section (Sect. 4) to the comparison between CFR and ADPFR results.

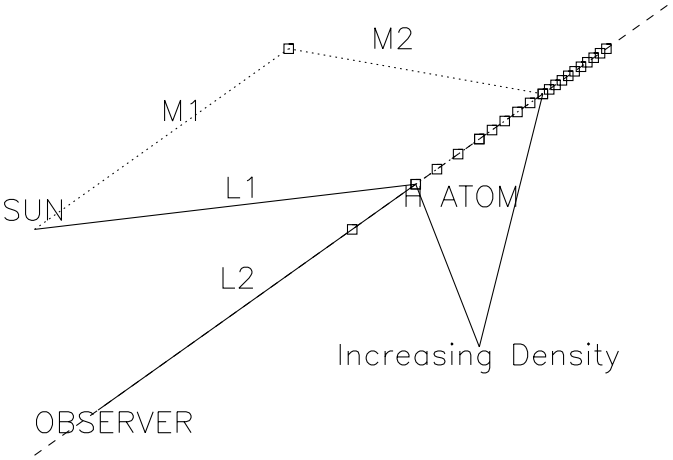

Fig. 3. Illustration of the scattering process of a Lyman alpha photon on a H atom in the heliosphere and its observation by an instrument in the heliosphere. The single scattering case is shown by the path L1 and L2. The multiple scattering case can be represented by M1, M2 and L2 but may involve more scatterings. The diamonds are used to show that the density increases with solar distance. This means that the thin medium of the inner heliosphere is surrounded by a denser medium which contributes to the intensity seen at 1 AU.

2.2.2. Terminology

This section tries to clarify the different terms used in what follows.

The physical quantities that can be measured are intensities. They correspond to a number of photons collected per surface unit per time unit per solid angle unit. Intensities are not local, they are integrated over a line of sight. Locally, the emissivity measures the number of photons emitted in all directions per volume unit per time unit. It can be divided into its spatial (per solid angle unit) and spectral (per frequency unit) components.

The only exact way to compute the interplanetary H Lyman α background requires a full computation of the multiple scattering process using an angle dependent partial frequency redistribution function. This must be coupled to a complete distribution of the density, velocity and temperature of the H atoms in the heliosphere. However, due to the complexity of the task, various approximations have been developed to speed up the computation.

In Fig. 3, we present a simple observing scenario. The intensity observed for a given Line Of Sight (LOS) is the integral over the line of sight of the local emissivity (Eq. (15) in Quémerais 2000). This emissivity is split in two terms. The *primary term* refers to photon which are scattered only once between the source and the observer (path L1+L2 in Fig. 3). The *secondary term* refers to photons that are scattered more than once (e.g. path M1+M2+L2 in Fig. 3). Many approximations neglect the secondary term. We will come back to that point later.

Approximations that neglect the secondary term:

- The first one is the *optically thin approximation* (noted OT). This corresponds to the assumption that extinction can be neglected and as a consequence that photons are scattered only once in the heliosphere. This assumption often gives correct intensity estimates in the inner heliosphere because extinction and multiple scattering tend to compensate one another (Keller et al. 1981; Hall 1992; Quémerais & Bertaux 1993). Its results tend to underestimate the line width in the case of the hot model (Quémerais 2000).
- The second type of computation is often referred to as the *primary intensity* (noted Primary here). It computes exactly the intensity due to single scattering, i.e. extinction is applied between the source and the observer. In the inner heliosphere, the primary term, noted I_0, represents roughly 60% of the intensity seen from 1 AU (Quémerais 2000). This may seem surprising since it is easy to remark that at one AU from the sun, the interplanetary medium is optically thin at Lyman α. However, we must not forget that the intensity is integrated over a large distance on the line of sight and that a significant fraction of the total intensity comes from outside the inner heliosphere where the medium is optically thicker.
- A third type of computation was used by Bertaux et al. (1985) to improve the accuracy of the optically thin case without going into the details of an actual radiative transfer computation. Is is often referred to as the self-absorbed computation (noted SA). It is identical to the optically thin calculation except that extinction on the line of sight between the scattering point and the observer is included. It is then an intermediate scheme between the optically thin case and the primary term which also includes extinction between the source and the scattering point.

Those three types of approximations can be used either with the CFR or the ADPFR redistribution function. Table 2 sums up the different hypotheses.

Following Quémerais (2000), we note that none of these numerical schemes fully represents the actual physical processes and that it is necessary to include all scattering orders to have a correct representation of the interplanetary Lyman α background. Numerical estimates of the errors introduced by these approximations are given in Quémerais (2000).

We will also repeat the remarks of Sect. 3 of Quémerais (2000). Scherer & Fahr (1996) and subsequent works claim that the secondary intensity term is negligible and that the primary term is enough to compute exactly the UV background in the inner heliosphere. We found that this is inexact here as already stated in Quémerais (2000).

It is clear that the interplanetary medium is optically thin at 1 AU. However, optical thickness increases with solar distance. At 10 AU, it is not optically thin anymore. Photons that cross the inner heliosphere are scattered at greater distance from the sun and a fraction of these contributes to the intensity seen at one AU. This is illustrated in Fig. 3.

More recently, Scherer & Scherer (2001) have considered the ratio of the backscattered intensity by He atoms at 58.4 nm with the resonance scattering of H atoms (121.6 nm) measured by the same instrument on Pioneer 10. They found that the ratio of both UV glow data is fairly constant over roughly 30 AU, between 1972 to 1984. From this remark and using the fact that the interplanetary medium is optically thin at 58.4 nm, they conclude that the H Lyman α UV glow can be modeled by

Table 2. Model approximation summary.

Approximation		noted	Extinction		Secondary term
			on L1	on L2	included
Optically Thin	(OT)	I_{ot}	No	No	No
Primary Term	(Primary)	I_0	Yes	Yes	No
Self-Absorbed	(SA)	I_{sa}	No	Yes	No

an optically thin approximation "because otherwise the ratio would not be constant for such a large heliocentric distance" (quote from Scherer & Scherer 2001, pages 137–138).

This last sentence is inexact. One of the most striking results of the various models of Keller et al. (1981), Hall (1992), Quémerais & Bertaux (1993) is that the intensity ratio of an optically thin model with a full radiative transfer model is roughly constant over a range of distances to the sun. The actual range of distance over which the ratio is more or less constant depends on the density model used in the model. This is due to a cancellation of effects between extinction and multiple scattering terms. A similar result is obtained by Quémerais (2000) (Fig. 8 of that paper) in the case of ADPFR. However, the value of the ratio is not the same if one considers observations in the upwind direction or the downwind direction. It is well known that the upwind to downwind intensity ratio is not correctly modeled by an optically thin approxmation (Keller et al. 1981; Quémerais 2000).

2.3. Model accuracy

In this section, we present estimates of the model accuracy and numerical stability. First we consider the radiative transfer Monte Carlo code. Second, we discuss error propagation between the Monte Carlo computation of hydrogen atom distributions and the Monte Carlo code used to compute the multiple scattering terms.

2.3.1. Radiative transfer Monte Carlo model

For the Monte Carlo model of multiple scattering, we simulate the path of a large number of photons emitted by the sun (Quémerais 2000). The local emissivity is obtained by keeping track of where the simulated photons are scattered and storing this information in a set of counters defined on a spatial and spectral grid. This means that at the end of the run, each grid point has counted a number of scatterings. The corresponding 1-σ statistical error for each counter is equal to the square root of the number of counts.

From this, we have derived the statistical error for each of the physical quantities used by applying the law of propagation of errors. This is expressed by

$$\sigma_f^2 = \sum_i \left(\frac{\partial f}{\partial x_i}\right)^2 \sigma_{x_i}^2 \qquad (1)$$

where the quantity f is a function of the independent variables x_i. σ_{x_i} expresses the individual statistical errors of the variables, σ_f is the statistical error of the derived quantity, i.e. emissivity or intensity in our case.

The model used in this work computed 160 million photon trajectories. The corresponding statistical accuracy is very good. The 1-σ statistical error for total intensities (i.e. integrated over spectral range) is everywhere lower than 5 Rayleighs. The corresponding model accuracies for total intensities vary between 1% to 5% according to the line of sight. In Fig. 6, we show the individual errors in each spectral bin.

The 1-σ statistical error for apparent line doppler shifts is smaller than 0.5 km s^{-1}. In most of the cases it is lower than than 0.2 km s^{-1} except for lines of sight close to the wind axis where the effective counter size is smaller.

Finally, apparent line temperatures have a 1-σ statistical error smaller than 1000 K everywhere. For most of the lines of sight, the error is smaller than 500 K except close to the axis of symmetry of the density model where it reaches 1000 K. Statistical errors for the temperature are shown in Fig. 9.

2.3.2. Error propagation between Monte Carlo models

The last question that arises from our model is the problem of numerical stability. The H atom density and velocity distribution is the result of a Monte Carlo computation (Izmodenov et al. 2001). As stated by these authors, the number density values have an accuracy better than 5%. From this we can deduce the accuracy of model intensities. It is clear that for the optically thin case, multiplying all densities by a factor k, changes the intensities by the same factor. The primary term is simply the optically thin case with extinction on the photon path. This means that all primary terms have a statistical accuracy of 5%.

However, we must also consider the effect of density inaccuracy in our computations of the secondary term due to multiple scattering. If the model is not numerically stable, a small change in density will yield a large change in multiply scattered intensity.

To test this, we ran three new MC models. The original model is noted MC0. A second model, noted MC1, is the same as the previous one except all densities have been multiplied by a factor 1.05. Similarly, MC2 is the same as MC0 except all densities are multiplied by a factor 0.95. Finally, a third attempt (MC3), is the same model as MC0, except densities are multiplied by random numbers between 0.95 and 1.05.

We then compared all secondary emissivities from the various models. It was found that the difference in secondary emissivities between MC1 or MC2 and MC0 is always smaller than 10% within 100 AU of the Sun. The difference of the secondary emissivity between MC2 and MC0 is much smaller, less than 2%. This proves that the model is numerically stable and that a small relative variation in density gives only a small variation in emissivity terms.

Finally, after integration over the line of sight, we found that the difference in secondary intensity between the different models is always less than 20 Rayleighs at 1 AU. This value corresponds to a rough estimate of the upper limit of the statistical error due to the combination of both Monte Carlo codes.

3. Observations at 1 AU

In this section, we present results obtained from our model computations. The first subsection shows that the three populations of H atoms have clearly distinct spectral features. Those features are averaged out for multiple scattered components of the intensity. In the second subsection, we present intensities, line shifts and line widths at 1 AU. The last part outlines the differences between the 3p model and the results of Quémerais (2000) obtained for the hot model.

3.1. Population study: example of the self-absorbed case

Before detailing the results of the 3p model, it is interesting to try and separate the different terms due to the three hydrogen populations. For this, we will consider only the first order of scattering. For higher orders of scattering the spectral features tend to be averaged over the different populations.

We have computed the line profiles in the case of the self-absorbed approximation (SA). The three moments, intensity, apparent velocity and apparent temperature can be computed for each of the populations and for the sum of the three components. For each of these computations, the observer is at 1 AU from the sun and is looking radially away from the sun.

Figures 4 and 5 show actual line profiles for both upwind and downwind directions. The HSWA population (dotted line) is much hotter than the other two populations. Although it is optically thin, it is slightly absorbed by the other two populations. The PIA component (dash-dot line) is faster than the HIA component (dashed line).

Tables 3 and 4 show the intensity, apparent velocity and apparent temperature for the self-absorbed line profiles as a function of the angle from upwind. Those values are also computed for each of the three populations. Although the HSWA component intensity is fairly small in the upwind direction (less than 5% of total), it represents a larger fraction in the downwind direction mainly because it is much more isotropic than the other two components. The slower component (HIA) is the one which is the more depleted in the downwind cavity because ionization processes are more effective for slower atoms in the solar rest frame.

Table 4 shows that the HSWA component is apparently much hotter than the other two components. When computing the line profile, we see that this component does not affect the center of the backscattered line but only contributes to the wings. In that sense, we will only consider the two cooler components when computing apparent temperatures in the rest of this work because they are the ones which correspond to line center photons. When computing apparent temperatures, we must give a temperature for the line center. Including the HSWA component term leads to overestimates of the line width because the actual profile is far from the Gaussian shape.

Table 3. Population study: self-absorbed intensity.

angle (°)	Total (R)	HSWA (%)	PIA (%)	HIA (%)
0	862	4.3	43.2	52.5
20	839	4.4	43.2	52.4
40	770	4.7	43.4	51.9
60	670	5.2	44.0	50.8
80	561	5.9	44.6	49.5
100	459	6.9	44.9	48.3
120	367	8.1	45.3	46.7
140	281	10.0	46.8	43.2
160	210	12.9	50.8	36.3
180	179	14.9	54.3	30.8

Table 4. Population study: SA lineshift and linewidth.

	Apparent velocity in km s^{-1}			
angle	Total	HSWA	HIA	PIA
0°	−28.18	−24.90	−24.63	−31.36
30°	−25.09	−23.27	−22.19	−27.65
60°	−16.59	−18.08	−15.38	−17.47
90°	−4.75	−10.64	−5.66	−3.14
120°	7.24	−2.98	4.64	11.53
150°	15.49	2.59	12.70	22.53
180°	17.64	4.84	15.84	27.03
	Apparent temperature in K			
angle	Total	HSWA	HIA	PIA
0°	17 590	18 1415	13 508	4928
30°	17 927	18 0469	14 187	5307
60°	19 817	18 3057	15 928	6154
90°	24 104	19 0651	18 085	6978
120°	30 475	20 0469	19 020	6981
150°	40 026	20 8312	17 718	6483
180°	48 744	21 1575	16 282	5902

3.2. Full radiative transfer computation

An example of a 3p full radiative transfer line profile is shown in Fig. 6. This has been computed for an observer at 1 AU crosswind from the sun and looking radially away from the sun. The primary term (sum of the three populations) is shown by the the dashed line. The total line is shown by the thick line and the secondary term, due to photons that have been scattered more than once between the sun and the observer, is shown by the dotted line. From Table 5, we see that the dotted line (secondary term) represents a bit more than 30% of the total intensity.

Table 5 gives the numerical values of the 3p total intensity, apparent velocity and apparent temperature as a function of the angle from the upwind direction. These values where obtained for a observer at 1 AU from the sun looking radially away from the sun. Note that, as stated above, the apparent temperature is computed using only the PIA and HIA populations which

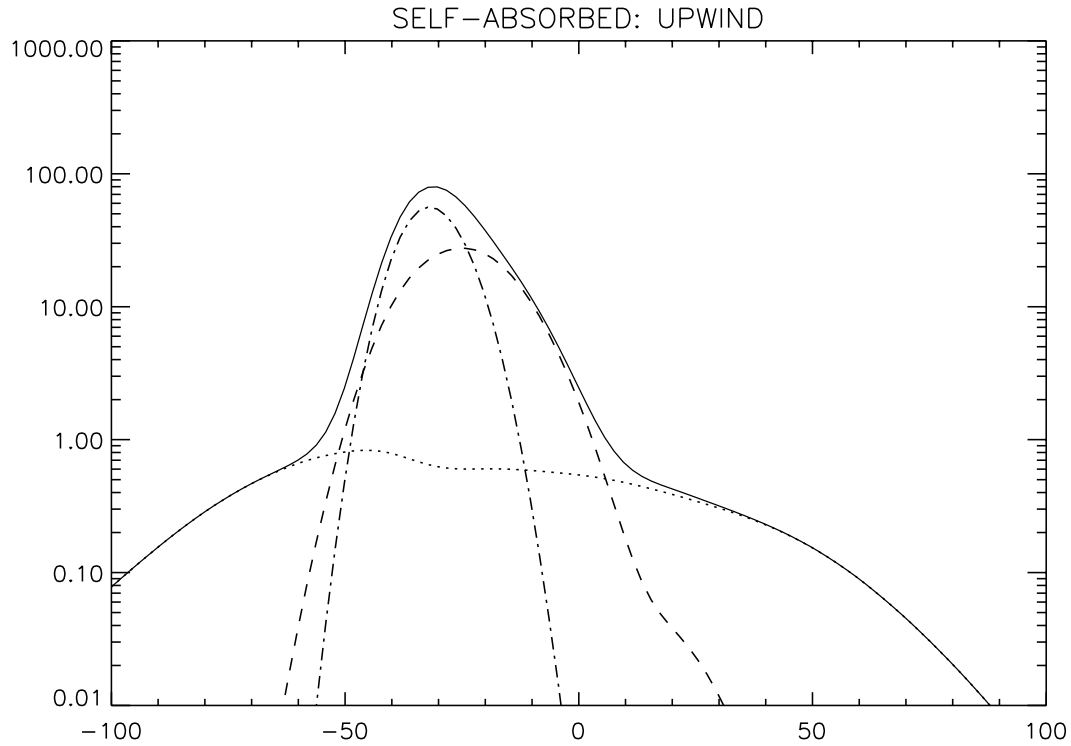

Fig. 4. Interplanetary line profile computed using the simple self-absorption approximation. The computation was made for an observer at one AU upwind from the sun looking in the upwind direction. The abscisse is in km s^{-1} in the solar rest frame and the ordinate is in units of rayleigh. The total line is shown by the thick solid line. The term due to the hot component is shown by the dotted line. The unperturbed interstellar component is shown by the dashed line. The component created at the interface is shown by dot-dashed line.

represent the temperature of the core of the line. Intensities and apparent velocities are computed using all three populations. The next three columns of Table 5 give the intensity ratio of the three approximations mentioned above with the total intensity. We have also compared the apparent temperatures obtained from the approximation with the apparent temperature obtained for the complete calculation. In general, the temperature obtained from the primary term is in good agreement with the apparent temperature found for the complete calculation, except in the upwind direction where the apparent temperature is underestimated. The self-absorbed case also gives a correct approximation. As usual is such computations, the optically thin case tends to underestimate the apparent temperature by roughly 15%, i.e. here by 1500 K. On the other hand, the optically thin case gives the best approximation for the total intensity. Note however that the upwind to downwind ratio is significantly changed by multiple scattering effects. This result was also observed in the case of the hot model by (Keller et al. 1981; Hall 1992; Quémerais & Bertaux 1993; Quémerais 2000). Multiple scattering effects tend to fill the downwind cavity when compared to the optically thin case. This decreases the contrast between the upwind and downwind directions.

The results of Table 5 are shown in Figs. 7–9. Figure 8 shows that the apparent velocity is not very sensitive to the way the background profile is computed. However, the optically thin case gives an approximation of the apparent velocity which is always within 1 km s^{-1} of the actual value. The other two approximations are within 3 km s^{-1}. In Fig. 9, we have displayed the apparent temperature of the line profiles as a function of the upwind direction. This apparent temperature corresponds to the sum of the two cooler populations, the PIA and HIA populations. We see in this figure that the full 3p calculation, the primary and self-absorbed calculations give very similar values in the downwind hemisphere. Yet the full 3p calculation is larger in the upwind direction, because it adds a component which is slower (less Doppler shifted) than the two primary components. In the upwind direction, the difference is roughly 1500 K. When comparing those data with optically thin or self-absorbed model computations, as done by Costa et al. (1999), one must roughly remove 1500 K to the observed value in the upwind direction to account for multiple scattering effects.

3.3. Differences with hot model results

Our interest here is to find ways to discriminate between interface models and hot models as seen from one AU. The reader is referred to Quémarais (2000) for the computation of the Hot model UV background results.

First, it must be pointed out that the main difference between the two types of models can be seen on the spectral profile of the backscattered line (Figs. 4–6). Indeed, the three-population type line profiles are much more dissymmetric than hot model line profiles. This is due to the existence of the faster unperturbed *lism component* and slower HIA component which are averaged in a unique population in the case of the hot model.

Furthermore, the existence of the hot component (HSWA) in the 3p model is a very obvious tool in this study. It has no

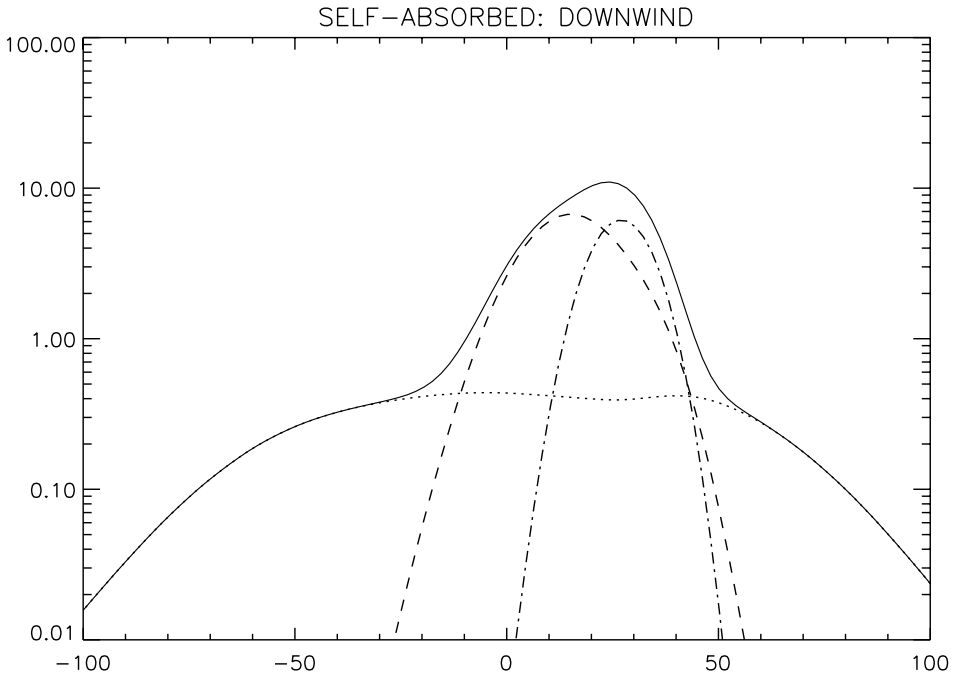

Fig. 5. Interplanetary line profile computed using the simple self-absorption approximation. The computation was made for an observer at one AU downwind from the sun looking in the downwind direction. The abscisse is in km s^{-1} in the solar rest frame and the ordinate is in units of rayleigh. The total line is shown by the thick solid line. The term due to the hot component is shown by the dotted line. The unperturbed interstellar component is shown by the dashed line. The component created at the interface is shown by dot-dashed line.

Table 5. Line profiles at 1 au from the sun.

θ (°)	I_n (R)	V_n (km s^{-1})	T_n (K)	$\frac{I_{ot}}{I_n}$	$\frac{I_0}{I_n}$	$\frac{I_{sa}}{I_n}$	$\frac{T_{ot}}{T_n}$	$\frac{T_0}{T_n}$	$\frac{T_{sa}}{T_n}$
0	1033	−27.3	11 608	1.08	0.75	0.83	0.87	0.89	0.88
10	1035	−27.0	11 436	1.07	0.74	0.83	0.88	0.90	0.89
20	1022	−26.0	11 478	1.06	0.74	0.82	0.88	0.90	0.89
30	986	−24.2	11 491	1.06	0.74	0.82	0.87	0.91	0.89
40	953	−21.9	11 471	1.05	0.73	0.81	0.88	0.92	0.90
50	896	−19.0	11 687	1.05	0.72	0.81	0.87	0.92	0.90
60	837	−15.6	11 929	1.04	0.72	0.80	0.87	0.93	0.91
70	785	−11.8	12 301	1.02	0.70	0.78	0.86	0.94	0.92
80	723	−7.8	12 715	1.01	0.70	0.78	0.86	0.96	0.93
90	666	−3.6	13 219	1.00	0.68	0.76	0.86	0.98	0.94
100	616	0.6	13 833	0.98	0.67	0.75	0.85	0.99	0.95
110	562	4.7	14 269	0.97	0.66	0.73	0.85	1.01	0.97
120	514	8.5	14 624	0.95	0.64	0.71	0.86	1.03	0.98
130	461	12.0	15 053	0.93	0.62	0.70	0.85	1.03	0.99
140	411	14.9	15 533	0.92	0.61	0.68	0.85	1.03	0.98
150	365	17.3	16 135	0.90	0.59	0.66	0.83	1.01	0.96
160	329	19.0	16 670	0.87	0.57	0.64	0.81	0.99	0.95
170	302	19.7	16 735	0.85	0.55	0.62	0.82	1.00	0.95
180	290	20.0	16 568	0.84	0.55	0.62	0.83	1.01	0.97

counterpart in the Hot model. This result will used to reanalyze the hydrogen cell measurements of the SWAN instrument which are very sensitive to doppler shift.

If we consider the intensity measurements, we note that the two types of models are very similar in the upwind hemisphere. The upwind to crosswind intensity ratio will not give any useful information. The upwind to downwind intensity ratio could be used here, unfortunately this requires to have a very good knowledge of the effective radiation pressure at the time of observation. Indeed, we know that changes of the radiation

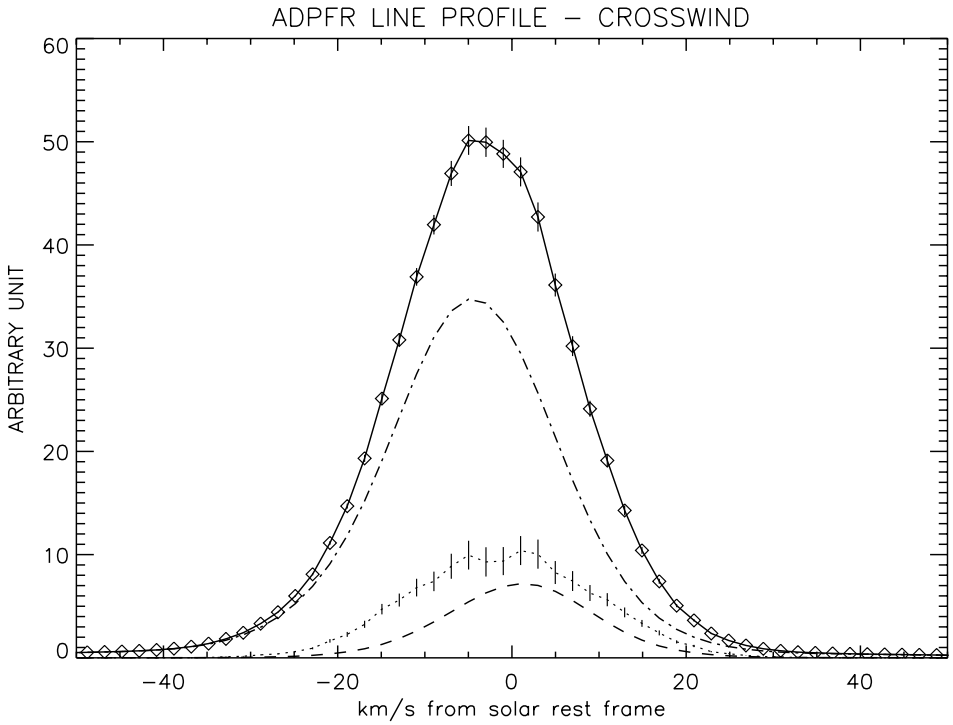

Fig. 6. Interplanetary line profile computed using the full angle dependent partial frequency redistribution model. The computation was made for an observer at one AU crosswind from the sun looking radially away from the sun. The abscisse is in km s^{-1} in the solar rest frame and the ordinate is in units of rayleigh. The total line is shown by the thick solid line. Statistical errors are shown. The primary term (sum of 3 primary components) is shown by the dash-dot line. The term due to photons scattered 2 times is shown by the dotted line. Finally, the term computed by the MC code for photons scattered more than two times is shown by the dotted line. The corresponding statistical errors are shown.

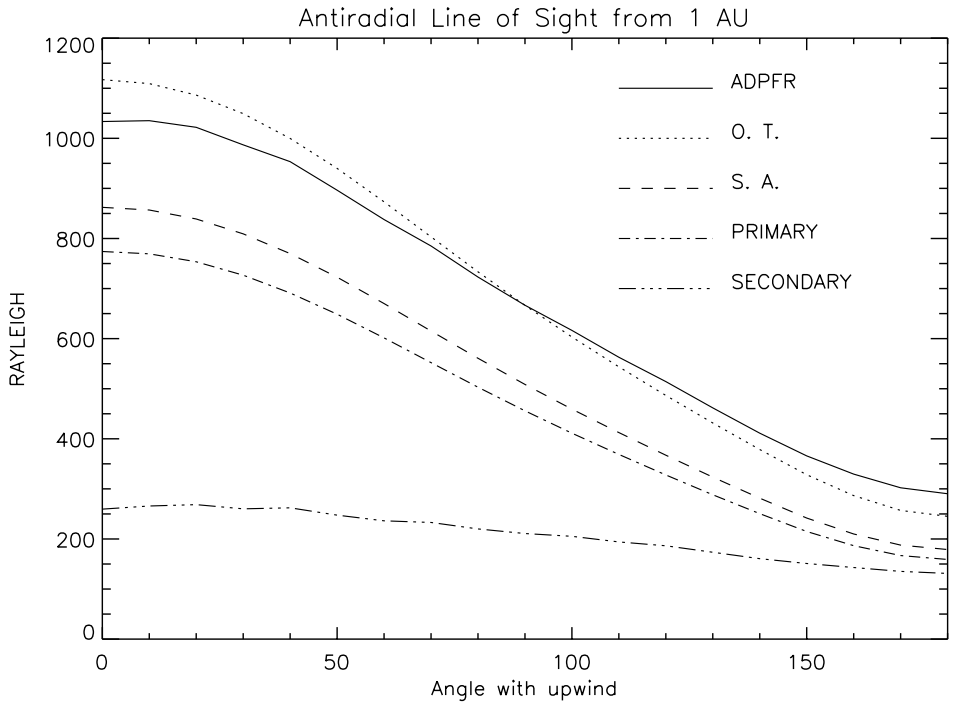

Fig. 7. Intensities from the 3p model as a function of the angle from the upwind direction. The full radiative transfer result is shown by the solid line. It is composed of the primary (dash-dot line) and secondary (3 dots and dash line) terms. For comparison we have added the optically thin result (dotted line) and the self-absorbed computation (dashed line).

pressure have effects on the upwind to downwind intensity ratio which are of the same order of magnitude as the one we are seeing between the two types of hydrogen distributions. This becomes even more difficult if we consider solar cycle

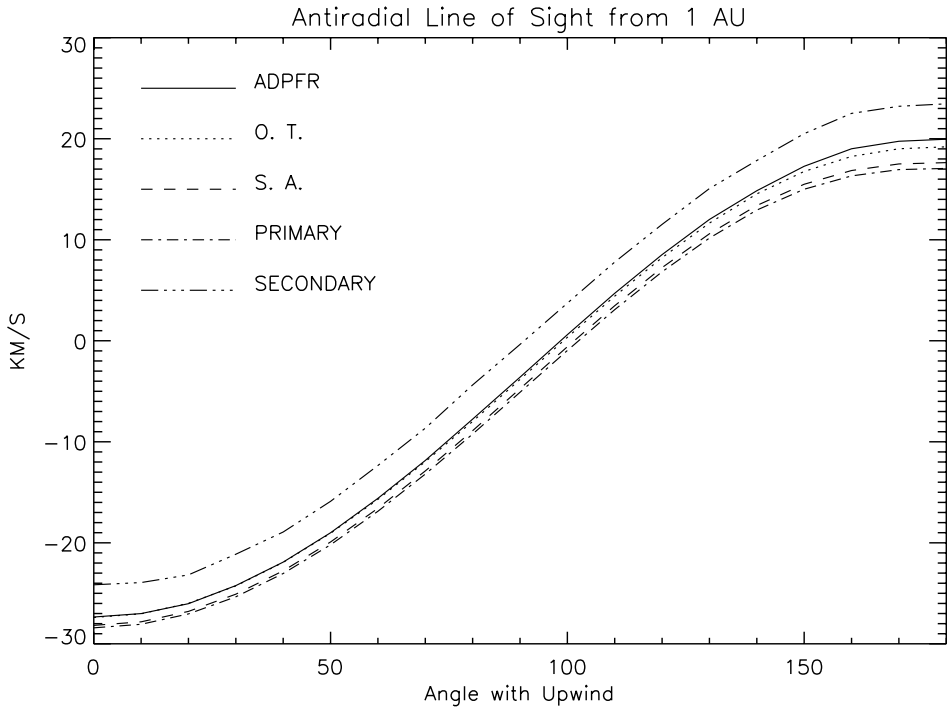

Fig. 8. Apparent velocity (line shift) as a function of the angle from the upwind direction from the 3p ADPFR model. The reference is the solar rest frame. As in the previous figure, we show the full radiative transfer result (solid line) as well as the result for primary and secondary terms. The optically thin result (dotted line) is very similar to the full computation line shift. Self-absorbed and primary results are very similar.In general line shifts are not very sensitive to the type of computation (ADPFR, OT or SA).

variation of the radiation pressure as shown by Bzowski et al. (2001). At the present time, the uncertainty on the actual radiation pressure from the sun does not allow us to discriminate between the two types of hydrogen models by simply studying the upwind over downwind intensity ratio. Let us note also that the apparent velocity is sensitive to the value of the radiation pressure.

Finally, we can compare the apparent temperature deduced from these models (Fig. 9). We see that the line width is larger in the downwind direction in the case of the existence of the heliospheric interface. However, the change is rather small (10%) and once again the uncertainty on the various interstellar and solar parameters will prevent an easy diagnostic from observations obtained at one AU from the sun. We can also note that the apparent temperature of the 3p model as a function of the angle with the upwind direction is almost constant within 50° of the upwind direction (see Fig. 9). This is not true for the hot model. In that second case, we find an increase of 600 K at 50° from the upwind value. A similar effect was described by Costa et al. (1999) from the study of hydrogen cell data. Further data analysis will be required to clarify this point.

4. Conclusion

In this work we have presented the results obtained by combining the hydrogen distribution model obtained by Izmodenov et al. (2001) which takes into account effects of the heliospheric interface with the full radiative transfer model described by Quémerais (2000). The main change applied to the interplanetary background model was to allow for the existence of three hydrogen populations, each with distinct local density, bulk velocity and projected temperatures.

This model has been applied to compute interplanetary background line profiles as seen by an observer at 1 AU from the sun. This study was compared to previous results of Quémerais (2000) obtained for a hot model of hydrogen distribution.

The most conspicuous difference between the hot model and three-population model computations is the existence for the latter type of model of a hot component (apparent temperature around more than 1.5×10^5 K) which does not exist in the case of the hot model. At 1 AU in the upwind direction, this component amounts to less than 5% of the total intensity. In the downwind direction, it represents up to 15% of the total intensity. Detecting this component would give a very strong proof of the existence and structure of the heliospheric interface. Use of the hydrogen cell data from the SWAN instrument will be made to try and detect this feature. High signal to noise measurements from the Hubble Space Telescope (Clarke et al. 1998) could also be useful here.

Other effects on the line profile as seen from one AU are harder to use to discriminate between the two types of hydrogen distributions. The main reason is that time-dependent variations of the solar parameters (radiation pressure for instance) induce changes in the hydrogen distribution in the inner heliosphere which are similar to those due to the interface. Thus a full model of the hydrogen distribution should include time-dependent variations of the solar parameters. Bzowski et al. (2001) developed an initial study for the hot model. We need to quantify the changes induced by solar cycle variations of the

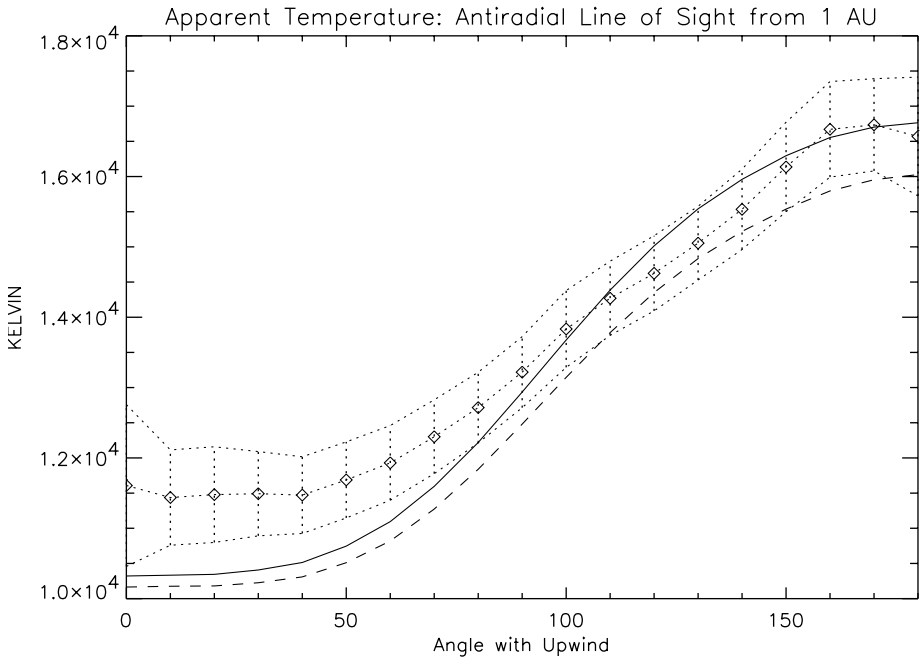

Fig. 9. Apparent temperature (line width) of antiradial line intensities (from 1 AU) as a function of the angle from the upwind direction. The full radiative transfer (3p ADPFR model) result is shown by the diamonds and dotted lines. The solid line corresponds to the primary term computation and the dashed line to the self-absorbed approximation. The statistical errors computed above are shown by the dotted line. The ADPFR model yields results similar to the Primary and Self-Absorbed cases in the downwind hemisphere but slightly larger (15%) in the upwind part of the sky.

solar parameters. Once this is done, we are confident that we will be able to discriminate between the different models from actual interplanetary line profile data.

Acknowledgements. This work was supported partly by INTAS grant 2001-0270. V.I. was also supported by the International Space Science Institute in Bern, and RFBR grants 01-02-17551, 02-02-06011 and 01-01-00759.

References

Ajello, J. M., Stewart, A. I. F., Thomas, G. E., & Graps, A. 1987, ApJ, 317, 964
Baranov, V. B., Lebedev, M. G., & Malama, Y. G. 1991, ApJ, 375, 347
Baranov, V. B., & Malama, Y. G. 1993, J. Geophys. Res., 98, 15157
Baranov, V. B., & Malama, Y. G. 1995, J. Geophys. Res., 100, 14755
Bertaux, J. L., & Blamont, J. E. 1971, A&A, 11, 200
Bertaux, J. L., Lallement, R., Kurt, V. G., & Mironova, E. N. 1985, A&A, 150, 1
Bertaux, J. L., Kyrola, E., Quémerais, E., et al. 1995, Sol. Phys., 162, 403
Brandt, J. C., & Chamberlain, J. W. 1959, A&A, 130, 670
Brasken, M., & E., Kyrölä 1998, A&A, 332, 732
Broadfoot, A. L., Sandel, B. R., Shemansky, D. E., et al. 1977, Space Sci. Rev., 21, 183
Bzowski, M., Summanen, T., Ruciński, D., & Kyrölä, E. 2001, J. Geophys. Res., in press
Clarke, J. T., Lallement, R., Bertaux, J.-L., et al. 1998, ApJ, 499, 482
Costa, J., Lallement, R., Quémerais, E., et al. 1999, A&A, 349, 660
Fukunishi, H., Watanabe, S., Taguchi, M., Okano, S., & Takahashi, Y. 1999, Adv. Space Res., 23(11), 1903
Hall, D. T. 1992, Ph.D. Thesis, University of Arizona, Tucson
Hall, D. T., Shemansky, D. E., Judge, D. L., Gangopadhyay, P., & Gruntman, M. A. 1993, J. Geophys. Res., 98, 15185
Hord, C., McClintock, W., Stewart, A. I. F., et al. 1992, Space Sci. Rev., 60, 1, 503
Izmodenov, V., Geiss, J., Lallement, R., et al. 1999, J. Geophys. Res., 104, A3, 4731
Izmodenov, V. 2000, Ap&SS, 274, 55
Izmodenov, V., Gruntman, M., & Malama, Y. G. 2001, J. Geophys. Res., 106, A6, 10681
Keller, H. U., Richter, K., & Thomas, G. 1981, A&A, 102, 415
Lallement, R., Bertaux, J. L., & Dalaudier, F. 1985, A&A, 150, 21
Lemaire, H. P., Emerich, C., Curdt, W., Schuehle, V., & Wilhelm, K. 1998, A&A, 334, 1095
Linsky, J. L., & Wood, B. E. 1996, ApJ, 463, 254
Malama, Y. G. 1991, Ap&SS, 176, 21
Mihalas, D. 1970, in Stellar Atmospheres (W. H. Freeman & Co, San Francisco)
Quémerais, E., & Bertaux, J. L. 1993, A&A, 277, 283
Quémerais, E., Sandel, B. R., Lallement, R., & Bertaux, J. L. 1995, A&A, 299, 249
Quémerais, E., Malama, Y. G., Sandel, B. R., et al. 1996, A&A, 308, 279
Quémerais, E., Bertaux, J.-L., Lallement, R., et al. 1999, J. Geophys. Res., 104, Issue A6, 12585
Quémerais, E. 2000, A&A, 358, 353
Scherer, H., & Fahr, H. J. 1996, A&A, 309, 957
Thomas, G. E., & Krassa, R. F. 1971, ApJ, 134, 20
Thomas, G. E. 1978, Ann. Rev. Earth Planet. Sci., 6, 173
Woods, T., Tobiska, W. K., Rottman, G. J., & Worden, J. R. 2000, J. Geophys. Res., 10527, 195